DUST, CLOUDS, AND THE ATMOSPHERIC OPTICAL DEPTH RECORD OVER 5 MARS YEARS OF THE MARS EXPLORATION ROVER MISSION

M. T. Lemmon, *Texas A&M University, College Station, TX, USA (lemmon@tamu.edu)*, **M. J. Wolff**, *Space Science Institute, Boulder, CO, USA*, **J. F. Bell III**, *Arizona State University, Tempe, AZ, USA*, **M. D. Smith**, *NASA Goddard Space Flight Center, Greenbelt, MD, USA*, **B. Cantor**, *Malin Space Science Systems, San Diego, California, USA*, **P. H. Smith**, *University of Arizona, Tucson, Arizona, USA*.

Introduction:

Dust aerosol plays a fundamental role in the behavior and evolution of the Martian atmosphere. Atmospheric dust and clouds have a direct effect on both surface and atmospheric heating rates, which are basic drivers of atmospheric dynamics. In turn, the resulting atmospheric motions influence the distribution of the dust itself, thus setting up a complex feedback [*e.g.*, Newman *et al.*, 2002]. For example, the lifting of dust from the surface of Mars is a function of winds and atmospheric instability (i.e., turbulence) at and near the surface, both of which are influenced in turn by heating rates dependent of the amount of atmospheric dust loading. This type of non-linear feedback mechanism is suspected of determining whether in a given year Mars will see a global dust event or only an assortment of local to regional storms [*e.g.*, Rafkin, 2009].

In January 2004, a new era of surface-based atmospheric observations began with the arrival of the MER missions. The two rovers, MER-A (Spirit) and MER-B (Opportunity) landed shortly before the Southern autumn equinox in Gusev crater (14.57°S, 175.48°E) and in Meridiani Planum (1.95°S, 354.47°E), respectively. Although "mission success" was considered to be 90 sols (a sol is a Martian solar day, about 1.0275 Earth solar days) for each rover, Spirit functioned through sol 2209 and Opportunity has accumulated more than 3000 sols as of this writing. Throughout their mission, the rovers have provided atmospheric optical depth measurements though direct solar imaging [Lemmon *et al.*, 2004]. The evolving optical depth data set (Fig. 1) has been used in coordinated ("ground truth") and contextual observations of the atmosphere and surface. In addition, this dataset has been applied to investigations of surface activity, photometric models investigating surface or atmospheric properties, and as inputs to discussions of chemical properties or biopotential.

Observations:

The MER atmospheric optical depth archive spans more than 2000 sols for Spirit and more than 3000 sols for Opportunity. The mission began near the end of Mars year (MY) 26, using the Clancy *et al*. [2000] convention for numbering mars years. In this work, we consider the entire Spirit data set and the Opportunity data set through the northern spring

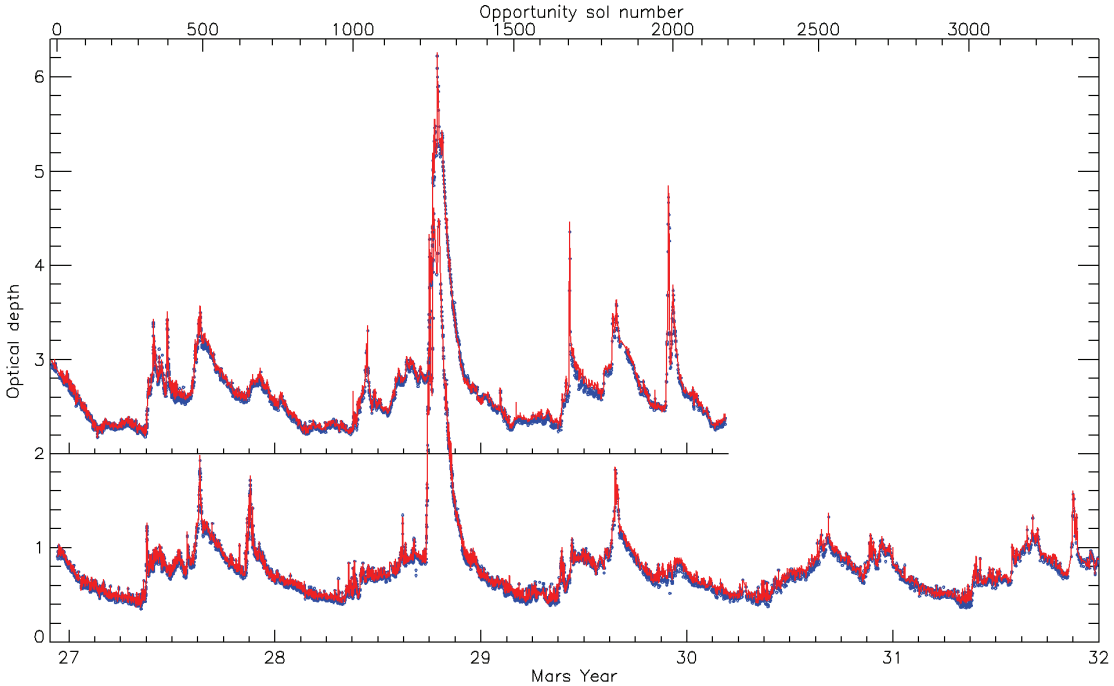

Figure 1. The MER optical depth record for Opportunity and Spirit (offset by 2. Opacity observed in L8 (blue symbols) and R8 (red line) is shown. Mars year is 27.0 at northern spring equinox (L_S=0°, Opportunity sol 41) following landing and increases proportionally to L_S between successive northern spring equinoxes; minor ticks indicate 45° of L_S. A sol scale along the top axis indicates Opportunity sol number (20.5 less than Spirit sol number), which is non-linear in L_S.

equinox at the end of MY 31 (31 July 2013). Pancam solar images using two neutral-density (ND) coated filters form the fundamental measurements. Pancam has two cameras (eyes) per rover, each with a CCD detector, a filter wheel, and optics that map a 16°x16° field of view onto 1024x1024 pixels [Bell *et al.,* 2003]. The solar filters are filter number eight in each of the right and left Pancams. The nominal wavelengths are 440 nm (L8) and 880 nm (R8), but the L8 filter is significantly affected by a red leak.

Conversion of solar images into an optical depth measurement is fundamentally simple: following the Beer-Lambert law, $F = F_{TOA} \bullet e^{-\tau \bullet \eta}$, where F is the measured flux, F_{TOA} is the top-of-atmosphere flux, τ is the desired normal-incidence optical depth, and η is the airmass, or ratio of slant-path optical depth to normal optical depth. Derivation of atmospheric transmittance, F/F_{TOA}, was done via a relative calibration approach [Smith and Lemmon, 1999]. Time variations in calibration are interpreted as dust accumulating on and eroding from the windows.

Discussion:

Figure 1 shows the optical depth record of the mission. Values in both filters are nearly the same: values discussed in this section are from R8 (880-nm) unless specified otherwise. The rovers' initial 90-sol mission included the southern autumnal equinox (L_S=0°) that began MY 27, during a time of moderate but declining optical depths. Spirit optical depths declined from near 0.90 to below ~0.3 by sol 155 (L_S=45°), and remained similarly low until about sol 350 (LS=135°). During this time, Opportunity optical depths declined from 0.95 to below ~0.5. The sudden increase of optical depth over L_S=135-137° was an operational surprise. It occurred in the last week of 2004, during a time of reduced staffing and was first seen as the first major reduction in solar power of the mission: an optical depth 1.24 dust storm peaking over sols B/329-332. Both rovers experienced local dust storms with optical depths of 1-1.5 and generally elevated optical depths from L_S 135° to 200°. Near L_S=215-220°, a period of rising opacity was seen first at the Spirit site, but briefly peaked at optical depth 1.98 at the Opportunity site on B/492, as cross-equatorial storms created a second planet-encircling haze [Cantor, 2007]. Optical depths fell gradually until L_S=307° before the next wave of cross-equatorial storms increased opacity to 1.76 on sol B/630 (L_S=316.5°) and eventually encircled the planet.

Subsequent Mars years were broadly similar, with the exception of globally extensive dust storms around L_S=270° of MY 28. Figure 2 shows optical depths for all years in their seasonal context. The optical depths generally match orbital climatology from imaging and infrared opacity, which show low optical depths through southern winter, receding cap-edge dust storms leading to an increase in dust after L_S=135°, and regional storms around L_S=220° and 315° [Smith 2004, 2009; Wang 2007].

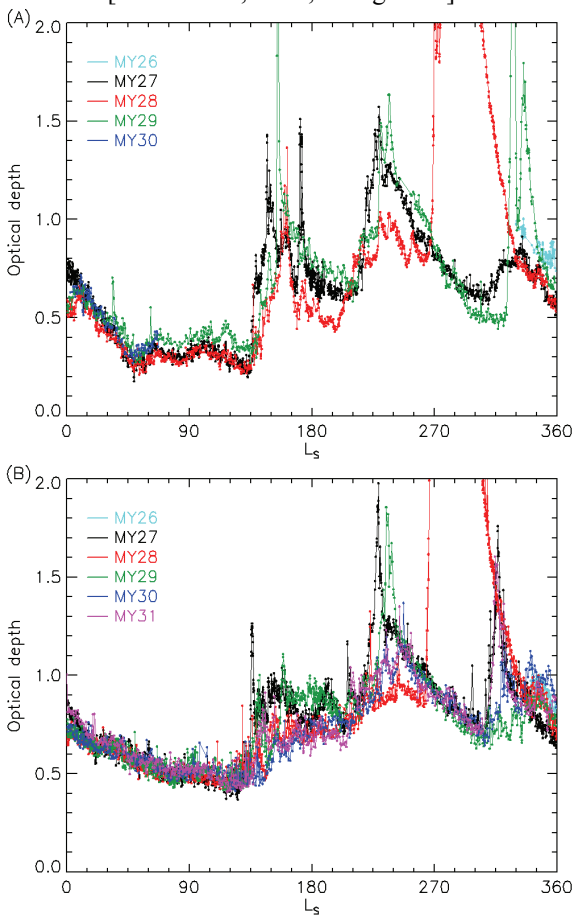

Figure 2. 880-nm optical depths as a function of season. Shown are results from (A) Spirit and (B) Opportunity for Mars years 26 (cyan, L_S>330 only), 27 (black), 28 (red), 29 (green), 30 (blue), and 31 (magenta). The 2007 dust storm is cut off to show detail at other times.

MY 28 is distinguished by a steady and low optical depth around L_S=215-265°, followed by a rapid increase beginning at L_S=265° (26 June 2007). This storm led to optical depths up to 4.27 at the Spirit site, where the optical depth was about 3 or more for a 30-sol period and rover operations were dramatically slowed by lack of available power. At the Opportunity site, the observed peak optical depth of 4.6 occurred on sol 1235 (L_S=277, 16 July 2007), after which the rover was commanded to hibernate to slow the drain of the batteries. The next observations, on sols 1243 and 1246, showed optical depths down to 3.9 and then back up, to eventually reach 4.5 and then slowly decline. The initial rate of decrease is 2.3-2.4%/sol, before the decrease slows and the optical depths become similar to those from other years.

Seasonal variations in dust aerosols. For the first part of the mission we have measurements of 9-μm dust opacity from Mini Thermal Emission Spectrometer (Mini-TES) data, as reported by Smith *et al.* [2004, 2006]. The record was continued through

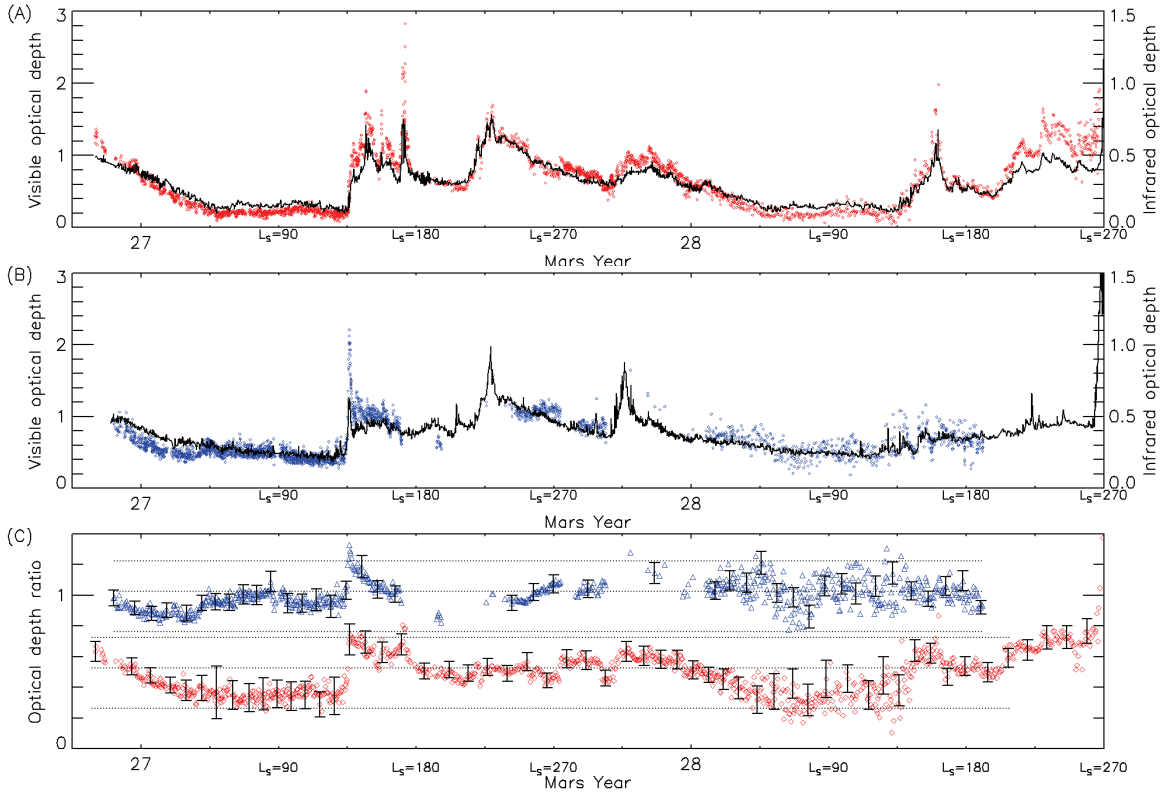

Figure 3. Visible to infrared opacity comparison. (A) The 0.88-μm (R8) opacity (black line) is compared with dust opacity observed by MiniTES at 9-μm (red diamonds, see Smith *et al.* [2006]). Uncertainties, not shown, are typically small compared to the symbols. (B) The same is shown for Opportunity, in blue. (C) The ratio of MiniTES to R8 opacity is shown; every 20th error bar is plotted. Opportunity values are offset by 0.5. The dotted lines correspond to aerosol sizes of 0.7, 1.4, and 2.1 μm, from bottom (see text).

the middle of MY 28 before dust on the Mini-TES optics rendered the data useless. Figure 3 shows the Mini-TES data with the 880-nm data for both rovers—note the infrared opacity scale is half the visible scale to generally overlay the data. The infrared/880-nm ratio is shown in Fig. 3C. There are clear trends: after landing, the ratio falls for both rovers; the ratio increases significantly with the onset of dust storms; the ratio tends to decline after dust storms and generally increases again for new storms; the ratio then falls for the next northern summer and rises with the second dusty season.

The comparison of these optical depths can be informative as to dust aerosol size [Clancy *et al.* 2003; Wolff *et al.* 2006]. For certain assumptions about IR optical properties of dust, Wolff *et al.* [2006] derived the (inverse) ratio as a function of mean size and variance of the size distribution. Based on their Fig. 13 and assuming a variance of 0.5, in Fig. 3C we show the ratio for mean radii of 0.7, 1.4, and 2.1 μm for both rovers. For different assumptions, those sizes would change, but the approximate relation would remain. The Opportunity data around L_S=30-130° are somewhat problematic: the 880-nm value is a total optical depth; the Mini-TES value is specific to dust. Mini-TES did not detect water ice, but orbital data show ice at that time, and the Mini-TES data do not rule ice out at high altitude [Smith *et al.* 2006]. So, the ratio may be depressed due to ice hazes. Generally, dust sizes fall as low as ~1 μm in northern summer and increase to over 2 μm with the onset of a dust storm (given the caveat above). This pattern is similar to patterns reported by Clancy *et al.* [2003] using orbital infrared spectroscopy.

Clouds. The Spirit and Opportunity opacity records are quite similar. An exception is the elevated opacity and occasional spikes during northern summer at the Opportunity site. The TES climatology and contemporaneous orbital observations show near-equatorial ice aerosols [Smith 2004, 2009]. Initially, regular sky monitoring was done with the rovers' Navcams. Also, regular drive-direction imagery frequently showed the sky. Prior to sol B/100, no discrete clouds were noted. During sols B/101-109 (L_S~30°) and again in the 140s (L_S~50°), clouds were noted in several images, leading to the regular campaigns (Fig. 4). During the first Mars year, cirriform clouds were seen occasionally until sol B/310 (over L_S=50-126°), especially around L_S~55° and 115°. During the second year, cirriform clouds were seen over L_S=23-50° and L_S=110-131°. During the third year, sampling was more sparse, but such clouds were seen near L_S=20° and over L_S=109-136°, with a real gap in between. Such clouds are likely the reason for the small spikes in optical depth, but ice hazes may be more generally present.

The images are not diagnostic as to the composition. Water ice is likely, given the aphelion cloud belt over the Opportunity site. However, mesospheric carbon dioxide ice clouds have been seen near the Meridiani area, peaking near L_S=30 and 150° [Clancy *et al.*, 2007]. It is possible that some of the early-season clouds were CO_2 ice. No discrete ice clouds were seen at either site outside of L_S=20-136°.

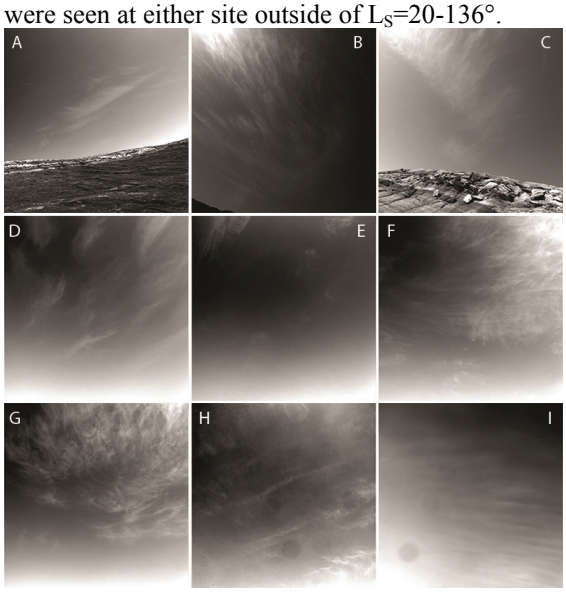

Figure 4. Opportunity Navcam images of clouds acquired on sol (A) 269, L_S=106°; (B) 290, 116°; (C) 291, 117°; (D) 758, 24°; (E) 763, 27°; (F) 949, 112°; (G) 950, 112°; (H) 1647, 126°; and (I) 2847, 63°. All images have a linear contrast-stretch; clouds are typically near 15% contrast at their peak, except for (B) 30% and (I) 5%.

Seasonal variations in insolation and dust devils. Heating of the surface and atmosphere by sunlight is governed by both orbital parameters and atmospheric scattering. Mars has an eccentric orbit, with aphelion at 1.67 AU and perihelion at 1.38 AU. Thus, global average insolation at the top-of-atmosphere (TOA) varies by nearly 50%. The Opportunity site is nearly equatorial, so seasonal effects are dominated by the Sun being lower in the sky near the solstices. The Spirit site is still "tropical" in the sense of having the sub-solar latitude sweep over its latitude before and after summer solstice. However, it is sufficiently far south that the Sun is much lower in the sky in winter. The two effects are roughly in phase, with perihelion at L_S=251°, roughly 35 sols before summer solstice. We have modeled the solar fluxes at TOA, at the surface and absorbed into the atmosphere (Fig. 5). Even during the optical depth >4 dust storm, surface insolation only falls by a factor of ~2-3 (rather than ~100 for direct sunlight) due to scattered light reaching the surface.

Greeley *et al.* [2010] discuss 3 Martian "dust devil seasons" that have happened during the 3 southern summers of the Spirit mission. Figure 5A shows their estimates of dust devil density. We have added error bars and upper limits based only on the counting statistics reported in Greeley *at al.* [2010, Fig. 3]. We note that at the Spirit site, dust devil frequency seems to increase exponentially with surface insolation (a similar fit could have been achieved for noon insolation or for the surface-atmosphere difference). The model fits both the seasonal change and the effect of the 2007 dust storms.

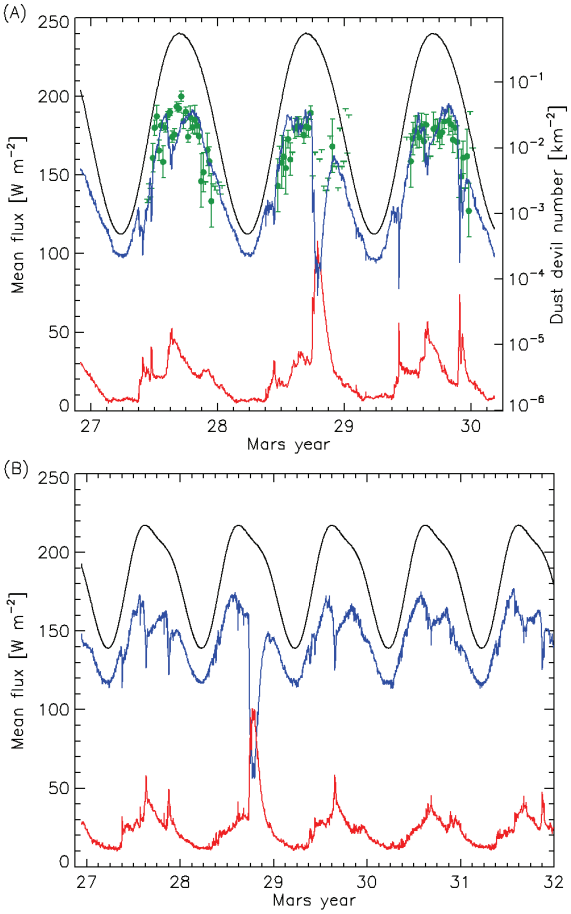

Figure 5. Insolation at the rover sites for (A) Spirit and (B) Opportunity. The continuous curves show modeled top-of-atmosphere, sol-average insolation (upper, black), direct plus diffuse surface insolation (middle, blue) and atmospheric absorption of sunlight (lower, red). For Spirit, symbols (green) show dust devil number density (right axis) reported by Greeley *et al.* [2010] with ⊤ symbols indicating upper limits.

References: Bell *et al.,* 2003, *J. Geophys. Res.*, **108**(E12), 8063. Cantor, 2007, *Icarus*, **186** 60-96. Clancy *et al*. 2000, *J. Geophys. Res.*, 105, E4. Clancy *et al.* 2003, *J. Geophys. Res.*, **108**, E9, 5098. Clancy *et al.*, 2007, *J. Geophys. Res.*, **112**, E04004. Greeley *et al.* 2010, *J. Geophys. Res.*, **115**, E00F02. Lemmon *et al.*, 2004, *Science*, **306**, 1753–1756. Newman *et al.*, 2002, *J. Geophys. Res.*, **107**(E12), 5124. Rafkin, 2009, *J. Geophys. Res.*, 114, E01009. Smith 2004, *Icarus,* **167**, 148-165. Smith 2009, *Icarus,* **202**, 444-452. Smith and Lemmon, 1999, *J. Geophys. Res.*, 104(E4), 8975–8985. Smith *et al.* 2006, *J. Geophys. Res.,* **111**, E12S13. Wang 2007, *Icarus* **189**, 325-343. Wolff *et al.* 2006, *J. Geophys. Res.*, **111**, E12S17.